Acta Oceanol. Sin., 2018, Vol. 37, No. 11, P. 53–60
DOI: 10.1007/s13131-018-1146-z
http://www.hyxb.org.cn
E-mail: hyxbe@263.net

Modeling of normal faulting in the subducting plates of the Tonga, Japan, Izu-Bonin and Mariana Trenches: implications for near-trench plate weakening

ZHOU Zhiyuan[1], LIN Jian[2, 1]*, ZHANG Fan[3]

[1] Key Laboratory of Ocean and Marginal Sea Geology, South China Sea Institute of Oceanology, Chinese Academy of Sciences, Guangzhou 510301, China

[2] Department of Geology and Geophysics, Woods Hole Oceanographic Institution, Woods Hole, Massachusetts 02543, USA

[3] Department of Ocean Science and Engineering, Southern University of Science and Technology, Shenzhen 518055, China

Received 29 March 2018; accepted 26 April 2018

Abstract

The plate flexure and normal faulting characteristics along the Tonga, Japan, Izu-Bonin and Mariana Trenches are investigated by combining observations and modeling of elastoplastic deformation of the subducting plate. The observed average trench relief is found to be the smallest at the Japan Trench (3 km) and the largest at the Mariana Trench (4.9 km), and the average fault throw is the smallest at the Japan Trench (113 m) and the largest at the Tonga Trench (284 m). A subducting plate is modeled to bend and generate normal faults subjected to three types of tectonic loading at the trench axis: vertical loading, bending moment, and horizontal tensional force. It is inverted for the solutions of tectonic loading that best fit the observed plate flexure and normal faulting characteristics of the four trenches. The results reveal that a horizontal tensional force (HTF) for the Japan Trench is 33%, 50% and 60% smaller than those of the Mariana, Tonga and Izu-Bonin Trenches, respectively. The normal faults are modeled to penetrate to a maximum depth of 29, 23, 32 and 32 km below the sea floor for the Tonga, Japan, Izu-Bonin and Mariana Trenches, respectively, which is consistent with the depths of relocated normal faulting earthquakes in the Japan and Izu-Bonin Trenches. Moreover, it is argued that the calculated horizontal tensional force is generally positively correlated with the observed mean fault throw, while the integrated area of the reduction in the effective elastic thickness is correlated with the trench relief. These results imply that the HTF plays a key role in controlling the normal faulting pattern and that plate weakening can lead to significant increase in the trench relief.

Key words: normal fault, geodynamic model, plate weakening, flexural bending, elasto-plastic deformation

Citation: Zhou Zhiyuan, Lin Jian, Zhang Fan. 2018. Modeling of normal faulting in the subducting plates of the Tonga, Japan, Izu-Bonin and Mariana Trenches: implications for near-trench plate weakening. Acta Oceanologica Sinica, 37(11): 53–60, doi: 10.1007/s13131-018-1146-z

1 Introduction

The subduction zone is a critical component of the earth's recycling system. During subduction, a downgoing plate sinks into the deep mantle and bends in response to its plate flexure, producing an extensional stress in the upper plate and a compressional stress in the lower plate (e.g., de Bremaecker, 1977; Hilde, 1983; Melosh, 1978; Parsons and Molnar, 1976). Numerous studies have revealed that the normal faulting caused by plate bending in the subduction zones plays an important role in upper mantle serpentinization, intraplate earthquakes, fluid flows in the plate, and tsunamis induced by outer-rise faulting (e.g., Christensen and Ruff, 1983; Kobayashi et al., 1998; Lefeldt et al., 2012; Masson, 1991; Ranero et al., 2003, 2005).

The normal faulting earthquakes in the subduction plates often occur close to coastlines and can thus pose great tsunami threat. In 1933, for example, a M_w 8.4 earthquake at the Japan Trench, which is the largest magnitude of an outer-rise normal faulting earthquake ever recorded, triggered a tsunami in the coastal area of Sanriku, Japan (Kanamori, 1971; Kao and Chen, 1996). In September 29, 2009, a M_w 8.1 outer-rise normal faulting earthquake occurred at the Tonga Trench and triggered a devastating tsunami (Beavan et al., 2010; Lay et al., 2010). Therefore, it is of great importance to study the dynamic mechanism of normal faulting in the subducting plate.

The normal faults have been observed to be pervasive between the outer rise and the trench axis. Observations revealed that the bending-related normal faults might be reactivated abyssal hill faults that formed at mid-ocean ridges or new faults that were generated during plate bending (Masson, 1991). Numerical modeling and analogue studies have inferred that the

Foundation item: The National Natural Science Foundation of China under contract Nos 41706056, 91628301 and U1606401; the Program of Chinese Academy of Sciences under contract Nos Y4SL021001, QYZDY-SSW-DQC005, YZ201325 and YZ201534; the Natural Science Foundation of Guangdong Province of China under contract No. 2017A030310066; the China Ocean Mineral Resources R & D Association under contract No. DY135-S2-1-04.
*Corresponding author, E-mail: jlin@whoi.edu

normal faults start to form at a distance from the trench axis, where the maximum stresses reach first and then grow toward the trench axis (Naliboff et al., 2013; Supak et al., 2006; Zhou et al., 2015).

Many deep trenches are located in the western Pacific, including the Tonga, Japan, Izu-Bonin and Mariana Trenches. There are large variations in the tectonic characteristics of these subduction zones, including trench depth, subduction dip angle, intra- and inter-plate seismicity, making them ideal for studying trench dynamics and plate interactions. More importantly, high-resolution bathymetry data are available for these trenches, making it possible to investigate fine-scale faulting characteristics.

In this study, we first quantified the plate bending flexure and normal faulting characteristics of the subducting plate along the Tonga, Japan, Izu-Bonin and Mariana Trenches using high-resolution multibeam bathymetry data. We then modeled the development of the normal faults as elasto-plastic deformations in the subducting plate. Finally, by comparing the modeling results with the observations, we inverted to obtain the best-fitting solutions of tectonic loading along these trenches and calculated the reduction in effective elastic plate thickness due to plastic yielding and the development of the normal faults.

2 Normal faulting observations

The Tonga, Japan, Izu-Bonin and Mariana Trenches are all located in the western Pacific and have relatively old (more than 100 Ma) subducting plates, implying that the initial plate thickness might be relatively large and varies only slightly among the four trenches. Therefore, it is advantageous to compare their normal faulting characteristics to reveal their common features.

The normal faulting characteristics, including fault throw and density, are the results of plastic yielding during plate bending. We investigated the average fault throw and density from the high-resolution multibeam bathymetry data which were obtained from the multibeam bathymetry database (MBBDB) of the NOAA National Centers for environmental information and the global multi-resolution topography synthesis of the marine geoscience data system (Fig. 1) (Ryan et al., 2009). We first identified the areas of abrupt slope changes as potential faults on 2-D topographic profiles, and then confirmed these faults on 3-D topographic maps. Finally, we digitized the top and bottom points of a fault to calculate the fault throw and density. The average resolution of the multibeam grid data is approximately 100 m. We extracted 14, 9, 15 and 15 across-trench profiles along the Tonga, Japan, Izu-Bonin and Mariana Trenches, respectively, to calculate the average fault throw and density. The profile locations were chosen manually considering the following factors: (1) availability of high-resolution multibeam data; (2) ensuring that the profiles are long enough (typically greater than 120 km) to include all of the visible faults on the topography; and (3) maintaining relatively uniform spacing between adjacent profiles.

The high-resolution multibeam bathymetry data reveal that the normal faults are pervasive at the four trenches (Fig. 1). The average fault throw at the Tonga Trench was observed to be the largest, with a maximum value of 420 m and a mean value of 284 m (Fig. 2a). The fault throws at the Izu-Bonin and Mariana Trenches were similar in size, with the same maximum value of 320 m and mean values of 238 and 148 m, respectively. The fault throw at the Japan Trench was the smallest, with a maximum value of 210 m and a mean value of 113 m. Identifiable faults were observed to initiate at 85, 80, 100 and 115 km from the trench axis at the Tonga, Japan, Izu-Bonin and Mariana Trenches, respectively.

The normal faults were observed to be most dense at the Mariana Trench and least dense at the Izu-Bonin Trench (Fig. 2b). The fault density started to increase significantly from 80 km from the trench axis at the Mariana Trench, but it started to increase at almost 50 km from the trench axis for all other trenches. This suggests that the normal faulting zone is the widest and the fault density is the greatest at the Mariana Trench.

3 Numerical modeling

A finite-element modeling software fast lagrangian analysis of continua (FLAC) (Cundall, 1989; Poliakov et al., 1993) was implemented to simulate the elasto-plastic deformation of the subducting plate. The FLAC incorporats a temperature- and strain-

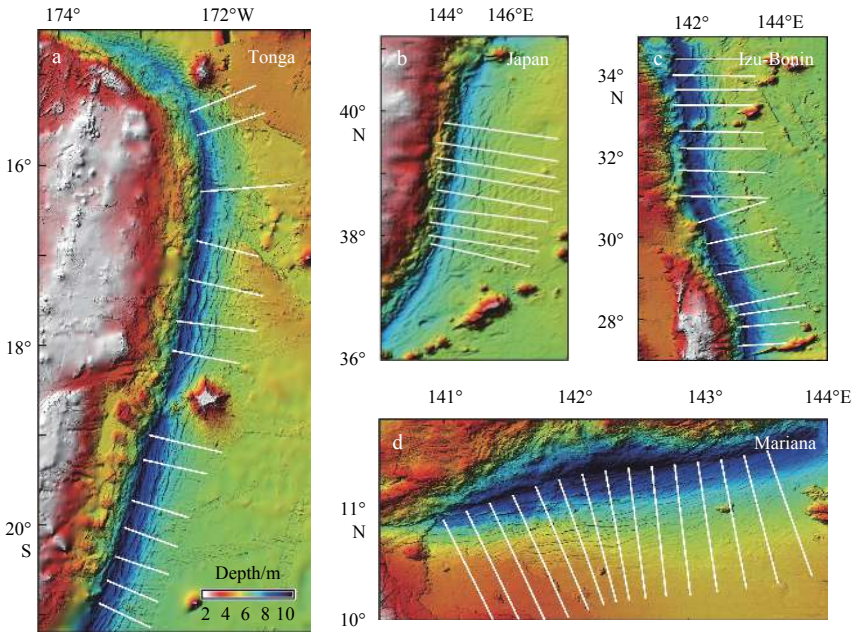

Fig. 1. Study regions with high-resolution bathymetry at the Tonga (a), Japan (b), Izu-Bonin (c) and southern Mariana (d) Trenches. The white lines indicate the analyzed profiles.

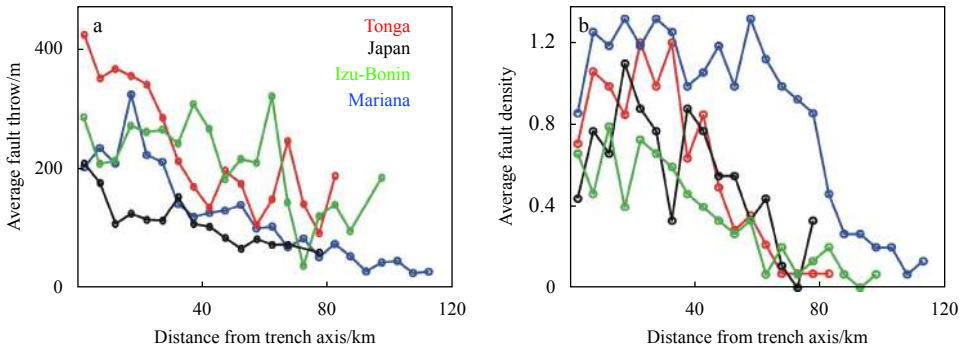

Fig. 2. The average fault throw (a) and fault density (b) per 5 km along the across-trench profiles at the Tonga, Japan, Izu-Bonin and Mariana Trenches.

rate-dependent visco-elastoplastic rheology and is capable of calculating the time-dependent stress and displacement fields at geological time scales (Buck and Poliakov, 1998; Lavier et al., 1999, 2000; Poliakov and Buck, 1998).

In our models, the lithosphere is assumed to be an elasto-plastic plate with an initial effective elastic thickness, and a substrate asthenosphere is modeled as a non-Newtonian Maxwell viscoelastic layer (Fig. 3a). A horizontal domain is 1 200 km. A vertical domain is 48 and 20 km, respectively, for the lithosphere and the asthenosphere. A horizontal mesh size is 0.5 km for the left 250 km, and 9.8 km for the right domain. A vertical mesh size is 0.5 and 2 km, respectively, for the lithosphere and the asthenosphere. The top surface is stress free, whereas the boundary between the lithosphere and the asthenosphere is subjected to a lithostatic pressure with zero shear stress. The left boundary, at the trench axis, is subjected to three types of tectonic loading: (1) a vertical loading V_0, (2) a bending moment M_0 and (3) a horizontal tensional force F_0 (HTF). The right boundary is fixed with zero displacement and is set at a sufficiently long distance to minimize its effects on the model domain.

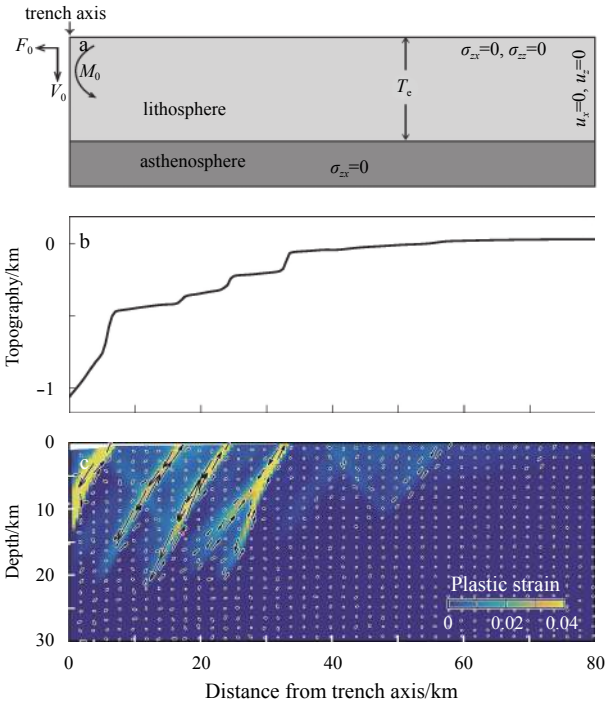

Fig. 3. Model setup and resulting topography, plastic strain, and relative velocity. a. Model setup and boundary conditions. An elasto-plastic lithosphere overlies a viscous asthenosphere. The top surface is stress free; tectonic loading is applied along the left boundary of the lithosphere; the right boundary is fixed with zero displacement; and the asthenosphere is subjected to lithostatic pressure with zero shear stress along the lithosphere-asthenosphere boundary; b. an example model of modeled topography; and c. modeled plastic strain and relative velocity illustrating the formation of normal faults under tectonic loading.

To minimize the effects of the substrate asthenosphere on the overriding lithospheric plate, we applied an abrupt temperature change from 450°C to 1 300°C at the boundary between the lithosphere and the asthenosphere. The Mohr-Coulomb yielding criterion was incorporated to produce plastic yielding of the brittle lithosphere (Jaeger and Cook, 1979): $\tau=C+\sigma\tan\phi$, where τ is the shear stress, C is the cohesion of the lithosphere, σ is a normal stress, ϕ is an internal friction angle, and $\mu=\tan\phi$ is the coefficient of friction. To facilitate the formation of the normal faults, we adopted a criterion that requires the cohesion to decrease with an increasing plastic strain. The initial cohesion C_0 was assumed to decrease linearly to a residual cohesion C_r before the plastic strain reaches a critical plastic strain ε_c. To facilitate the normal faulting in the subduction zone, we set a smaller value of the critical plastic strain relative to those used in previous studies of mid-ocean ridges (e.g., Behn and Ito, 2008; Buck et al., 2005; Poliakov and Buck, 1998). The other modeling parameters follow Lavier et al. (2000) (Table 1). We ran 735 model experiments with

Table 1. Model parameters

Parameter	Description	Value
T_e	initial plate thickness/km	48
E	Young's modulus/MPa	7.5×10^4
G	shear modulus/MPa	3.0×10^4
g	gravitational acceleration/m·s^{-2}	9.81
ν	Poisson's ratio	0.25
ρ	density/kg·m^{-3}	
τ	shear stress/MPa	
σ	normal stress/MPa	
μ	coefficient of friction	0.6
T	temperature/°C	0–1 300
V_0	vertical load/N·m^{-1}	
M_0	bending moment/N	
F_0	horizontal tensional force/N·m^{-1}	
C_0	initial cohesion/MPa	44
C_r	cohesion after faulting/MPa	4
ε_c	critical plastic strain	0.03

a combination of tectonic loads for comparison with the observations at the four trenches. The parameter space of the three types of tectonic loading includes the vertical loading in the range of 0–6.7×10^{12} N/m, the bending moment in the range of 0–1.2×10^{17} N, and the HTF in the range of 0–9.6×10^{12} N/m.

Our models predict the time-dependent topography (Fig. 3b) as well as the plastic strain and the relative velocity (Fig. 3c). It was observed that the normal faults in the subducting plate developed at various time frames under the tectonic loading and that the plastic strain accumulated through time. The models will eventually become steady-state when the whole system reaches equilibrium. The models predict a plate flexure and a fault distribution on the surface, which are used to compare with the observations.

4 Results

4.1 *Tectonic loading constrained by plate flexure and normal faulting*

The observed sea floor topography consists of various components, including sediment thickness, subsidence due to plate cooling, and Airy local isostatically compensated topography. Therefore, we approximated the plate flexure by using the non-isostatic topography (Zhang et al., 2014), in which all of the above effects were estimated and removed from the original topography (Figs 4a–d). We combined both the plate flexure and normal faulting characteristics to constrain the models and inverted for the best-fitting tectonic loading for the four trenches (Fig. 4). First, we calculated the root-mean-square (RMS) of the difference between the modeled topography and the observed plate flexure, which allows us to isolate a group of models with relatively smaller RMS values. This group of models with relatively smaller RMS was then compared with the observed fault throw distributions to further narrow down the best-fitting solutions.

The inverted best-fitting parameters for the four trenches are shown in Table 2. The results show that the vertical loading V_0 for the Tonga and Japan Trenches is 26% smaller than that for the Izu-Bonin and Mariana Trenches. The bending moment M_0 is significantly smaller for the Izu-Bonin Trench than it is for the other three trenches. Notably, there is a large variation in the horizontal tensional force F_0 among the four trenches. The HTF for the Japan Trench is 33%, 50% and 60% smaller than those for the Mariana, Tonga and Izu-Bonin Trenches, respectively.

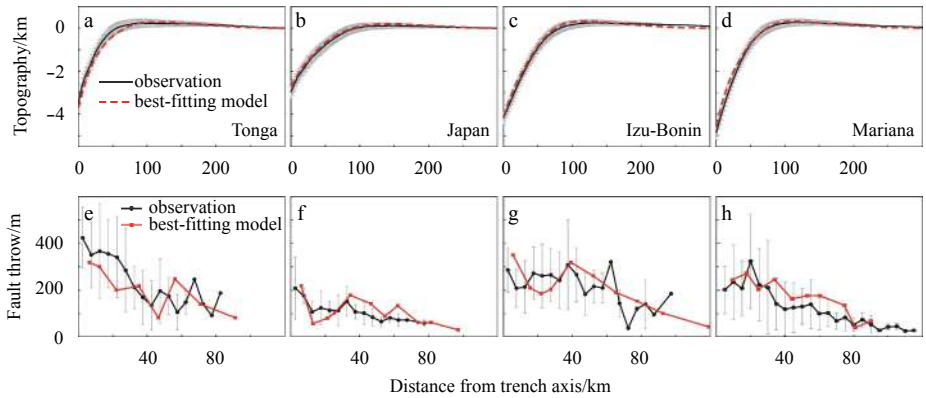

Fig. 4. Comparisons between the observed average non-isostatic topography (black lines) and best-fitting model topography (red lines) as a function of the across-axis distance from the trench axis (a–d), and comparisons of the fault throws between the observations (black curves) and the best-fitting models (red curves) (e–h). The gray lines indicate the errors in the observations.

Table 2. Comparisons of the model results for the Tonga, Japan, Izu-Bonin and Mariana Trenches

	Tonga	Japan	Izu-Bonin	Mariana
V_0/10^{12} N·m^{-1}	4.3	4.3	5.8	5.8
M_0/10^{16} N	9.6	7.7	3.8	9.6
F_0/10^{12} N·m^{-1}	4.8	2.4	6.0	3.6
W_0/km	3.5	3.0	4.2	4.9
Mean fault throw/m	284	113	238	148
Cumulative fault throw/m	2 993	1 118	1 714	3 121
Area of T_e reduction $S_{\Delta Te}$/km^2	1 120	1 028	1 143	1 289

Our models predicted the horizontal deviatoric stress in the subducting plate, which is directly responsible for the development of the normal faulting. There are two turning points in the depth profiles of the deviatoric stress: the boundary between the upper plastic yield zone and the middle elastic core and the boundary between the elastic core and the lower ductile zone (Fig. 5). The stress in the extensional yield zone generally increases with depth, except at locations with individual normal faults with fluctuating stresses. The stress varies almost linearly with depth in the elastic core from extensional to compressional and decreases abruptly to nearly zero in the ductile zone. The horizontal deviatoric stress at the Japan Trench is calculated to be consistently smaller than that of the other three trenches, which is consistent with the observation that both the mean and maximum fault throw values are the smallest at the Japan Trench.

4.2 *Reduction in effective elastic thickness*

Our models calculated the horizontal deviatoric stresses of the subducting plate during the evolution of plate bending. On the basis of the best-fitting models, the normal faulting patterns in the subducting plates for the four trenches are predicted (Figs 6a–d). The normal faults were calculated to develop within the upper plastic yield zone. The results reveal that most normal faults are dipping trenchward in the Japan, Izu-Bonin and Mariana Trenches but both trenchward and oceanward dipping faults are calculated for the Tonga Trench. The normal faults were calculated to be shallower in the Japan and Tonga Trenches than the Izu-Bonin and Mariana Trenches. The available relocated outer-rise normal faulting earthquakes within the study areas from Emry and Wiens (2015) are all located within the calculated extensional yield zone (Figs 6b and c).

On the basis of the calculated horizontal deviatoric stress, we

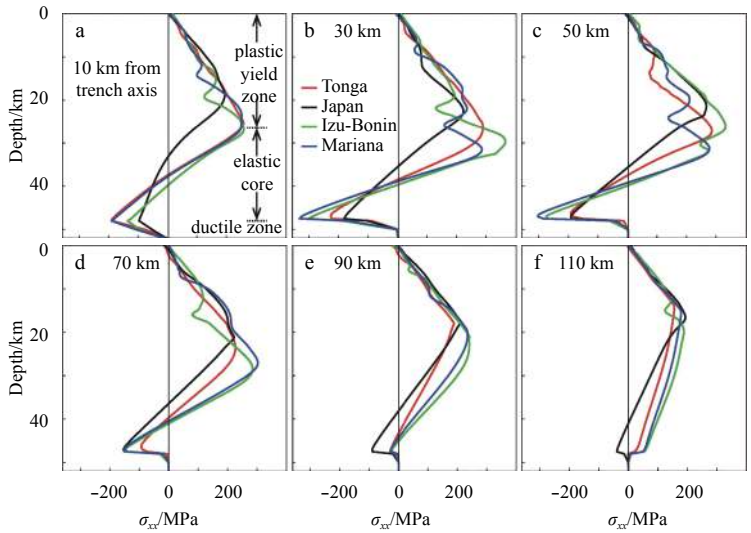

Fig. 5. The calculated horizontal deviatoric stress (σ_{xx}) as a function of depth, derived from the best-fitting models for the four trenches, at 10 km (a), 30 km (b), 50 km (c), 70 km (d), 90 km (e) and 110 km (f) from the trench axis.

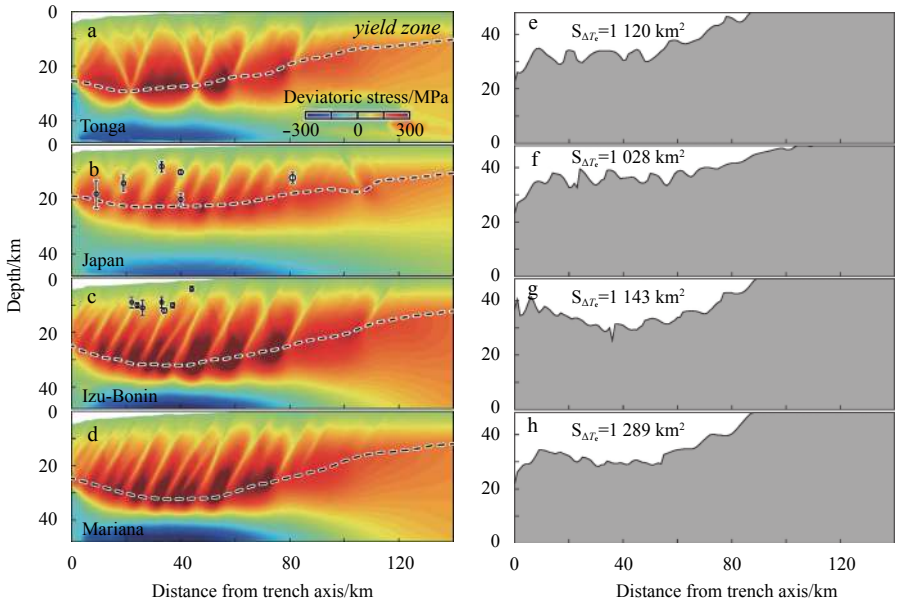

Fig. 6. Calculated horizontal deviatoric stresses and effective elastic plate thickness. a–d. Calculated horizontal deviatoric stresses of the models, illustrating the development of normal faults based on the best-fitting models for the Tonga, Japan, Izu-Bonin and Mariana Trenches, respectively. The dashed black curves denote the maximum depths of extensional yielding zones. The black circles with error bars show the available relocated outer-rise normal faulting earthquakes within the study area from Emry and Wiens (2015). e–h. The calculated T_e (black curves) and the calculated areas of T_e reduction SDT_e (white regions) for the four trenches.

calculated the resulting effective elastic plate thickness T_e due to plate bending and normal faulting (Figs 6e–h), following the methods of Hunter and Watts (2016) and Turcotte and Schubert (2014). The results reveal that the effective plate thickness decreases gradually toward the trench axis, with a maximum T_e reduction of 25, 24, 22 and 26 km at the Tonga, Japan, Izu-Bonin and Mariana Trenches, respectively. We then calculated the area of the T_e reduction $S_{\Delta Te}$ by integrating the T_e reduction over the across-axis distance. $S_{\Delta Te}$ was calculated to be the largest for the Mariana Trench and the smallest for the Japan Trench. Meanwhile, the width of the T_e reduction region was calculated to be the largest for the Japan Trench and almost the same for the other three trenches. Thus, the mean T_e reduction was the smallest for the Japan Trench and the largest for the Mariana Trench.

The observed trench relief W_0 is, on average, 3.5, 3.0, 4.2 and 4.9 km for the Tonga, Japan, Izu-Bonin and Mariana Trenches, respectively. The observed trench relief W_0 is generally positively correlated with $S_{\Delta Te}$ (Fig. 7a). This result implies that the plate weakening (i.e., $S_{\Delta Te}$) can lead to the significant increase in the trench relief.

5 Discussion

5.1 *Uncertainties in data analysis*

In this study, we have conducted comprehensive experimental runs with a large range of combinations of the three types of

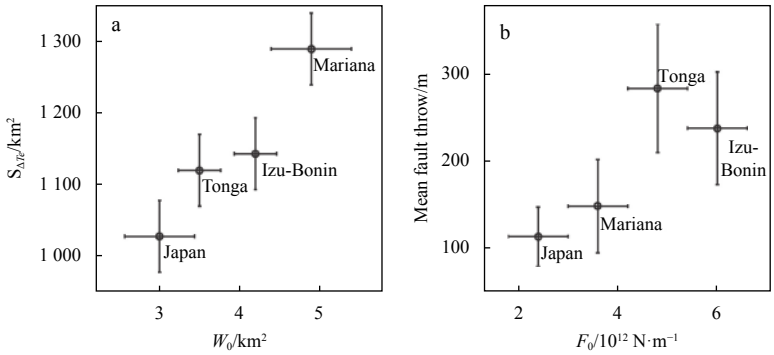

Fig. 7. The relationship between tectonic loading and observation. a. The relationship between the calculated area of T_e reduction SDTe and the observed trench relief W0, the error bars are shown as crosses; b. the relationship between the observed mean fault throw and the calculated horizontal tensional force F0.

tectonic loading to compare with the observations of plate flexure and normal faulting characteristics. As each model typically took tens of hours to complete, we have chosen reasonable parameter intervals to reach a balance between the model resolution and computational time: 0.48×10^{12} N/m for the vertical loading, 1.92×10^{16} N/m for the bending moment, and 0.6×10^{12} N/m for the HTF. Therefore, these parameter intervals were used as the error bars of the best-fitting models (Fig. 7). However, there are also uncertainties associated with the observations. We manually extracted profiles perpendicular to the trench axis and calculated their average values. Since there are large variations among the individual profiles, the error bars of the observed normal fault throws and plate flexure are relatively large (Fig. 4).

5.2 *Importance of horizontal tensional force*

Most of the studies that utilized the thin plate flexure theory have recognized the importance of the vertical loading and the bending moment. However, few studies have investigated the importance of the horizontal tensional force (e.g., Garcia-Castellanos et al., 2000; Zhou et al., 2015; Zhou and Lin, 2018). Our previous study reveals that the HTF is crucial for explaining both the plate flexure and the fault throw, particularly in controlling the across-axis distance of the maximum fault throw (Zhou et al., 2015). Here, we illustrate that the calculated HTF correlates positively with the observed mean fault throw of the four trenches (Fig. 7b). This result indicates that larger HTF facilitates the development of larger normal faults in the subducting plate. On the basis of the above results, we infer that the HTF plays a key role in controlling the normal faulting pattern. Since this study only investigated the subduction zones of relatively old plates, further studies are needed to test if the above inference still holds true for young subducting plates.

5.3 *Normal faulting depths and mantle serpentinization*

The normal faults in the subducting plate could provide potential channels for fluids penetrating into the crust and mantle, causing serpentinization of the upper mantle (e.g., Grevemeyer et al., 2005, 2007; Key et al., 2012; Ranero et al., 2003, 2005; Tilmann et al., 2008). Multi-channel seismic surveys have revealed that the bending-related normal faults can penetrate the Moho with a maximum depth of over 20 km below the sea floor (e.g., Han et al., 2016; Ranero et al., 2003; Ranero and Sallares, 2004).

From the calculated normal faulting patterns of the best-fitting models (Figs 6a–d), the normal faults could penetrate into maximum depths of 29, 23, 32 and 32 km below the sea floor for the Tonga, Japan, Izu-Bonin and Mariana Trenches, respectively. If we assumed a normal crustal thickness of 6 km, the calculated normal faults would cut through 23, 17, 26 and 26 km into the upper mantle for the four trenches, thus potentially causing massive mantle serpentinization.

We also calculated the cumulative down-dip fault lengths (i.e., the sum of the individual identifiable faults) to be 240, 260, 360 and 450 km for the Tonga, Japan, Izu-Bonin and Mariana Trenches, respectively. Through a seismic reflection study at the Cascadia Trench, Han et al. (2016) estimated the width of a water-penetrated fault zone surrounding an individual fault to be in a range of ~75–600 m. Assuming the same fault zone widths as Han et al. (2016), we estimated the volumes of the water-penetrated fault zone to be 18.0–144.0, 19.5–156.0, 27.0–216.0 and 34.0–270.0 km^2, yielding percentages of mantle serpentinization of 0.4%–3.4%, 0.4%–3.1%, 0.6%–5.1% and 1.4%–10.8% for the Tonga, Japan, Izu-Bonin and Mariana Trenches, respectively. This result implies that the degree of mantle serpentinization of the Mariana Trench may be significantly larger than that of the other three trenches, which is equivalent to 350% of both the Tonga and Japan Trenches and 230% of the Izu-Bonin Trench.

If the serpentine minerals near the fault zones in the mantle are chemically bound with 13 wt% water as suggested by previous studies (e.g., Faccenda, 2014; Ranero et al., 2003), then the serpentinized mantle regions would contain 0.052%–0.44%, 0.052%–0.40%, 0.078%–0.66% and 0.18%–1.40% mass fraction of water, which is equivalent to columns of 0.035–0.290, 0.026–0.200, 0.060–0.500 and 0.140–1.060 km of water per unit length of the trench axis of the Tonga, Japan, Izu-Bonin and Mariana Trenches, respectively. The above estimations are of the same order of magnitude as the estimations for the Cascadia Trench (0.023–0.18 km, Han et al., 2016) but are less than that for the Middle America Trench (0.17–1.7 km, Ranero et al., 2003).

6 Conclusions

(1) The tectonic loading for the Tonga, Japan, Izu-Bonin, and Mariana Trenches were inverted by comparing the observed plate flexure and normal faulting characteristics with the elastoplastic models, revealing that the horizontal tensional force for the Japan Trench is 33%, 50% and 60% smaller than that of the Mariana, Tonga, and Izu-Bonin Trenches, respectively.

(2) The normal faults were modeled to penetrate to a maximum depth of 29, 23, 32 and 32 km below the sea floor for the Tonga, Japan, Izu-Bonin and Mariana Trenches, respectively,

which is consistent with the depths of relocated normal faulting earthquakes in the Japan and Izu-Bonin Trenches and implies the significant serpentinization of an upper mantle layer.

(3) The calculated horizontal tensional force and the area of the effective elastic thickness reduction are in general positively correlated with the observed mean fault throw and trench relief, respectively, implying that the HTF plays a key role in controlling the normal faulting pattern and that the plate weakening can lead to the significant increase in the trench relief.

Acknowledgements

The authors are grateful to the staff and students of the deep sea geodynamics group of the South China Sea Institute of Oceanology, the Chinese Academy of Sciences for constructive discussion and suggestions.

References

Beavan J, Wang X, Holden C, et al. 2010. Near-simultaneous great earthquakes at Tongan megathrust and outer rise in September 2009. Nature, 466(7309): 959–963, doi: 10.1038/nature09292

Behn M D, Ito G. 2008. Magmatic and tectonic extension at mid-ocean ridges: 1. Controls on fault characteristics. Geochemistry, Geophysics, Geosystems, 9(8): Q08O10

Buck W R, Lavier L L, Poliakov A N B. 2005. Modes of faulting at mid-ocean ridges. Nature, 434(7034): 719–723, doi: 10.1038/nature03358

Buck W R, Poliakov A N B. 1998. Abyssal hills formed by stretching oceanic lithosphere. Nature, 392(6673): 272–275, doi: 10.1038/32636

Christensen D H, Ruff L J. 1983. Outer-rise earthquakes and seismic coupling. Geophysical Research Letters, 10(8): 697–700, doi: 10.1029/GL010i008p00697

Cundall P A. 1989. Numerical experiments on localization in frictional materials. Ingenieur-archiv, 59(2): 148–159, doi: 10.1007/BF00538368

De Bremaecker J C. 1977. Is the oceanic lithosphere elastic or viscous? Journal of Geophysical Research, 82: 2001–2004, doi: 10.1029/JB082i014p02001

Emry E L, Wiens D A. 2015. Incoming plate faulting in the northern and western Pacific and implications for subduction zone water budgets. Earth and Planetary Science Letters, 414: 176–186, doi: 10.1016/j.epsl.2014.12.042

Faccenda M. 2014. Water in the slab: A trilogy. Tectonophysics, 614(3): 1–30

Garcia-Castellanos D, Torne M, Fernàndez M. 2000. Slab pull effects from a flexural analysis of the Tonga and Kermadec Trenches (Pacific plate). Geophysical Journal International, 141(2): 479–484, doi: 10.1046/j.1365-246x.2000.00096.x

Grevemeyer I, Kaul N, Diaz-Naveas J L, et al. 2005. Heat flow and bending-related faulting at subduction trenches: Case studies offshore of Nicaragua and Central Chile. Earth and Planetary Science Letters, 236(1–2): 238–248, doi: 10.1016/j.epsl.2005.04.048

Grevemeyer I, Ranero C R, Flueh E R, et al. 2007. Passive and active seismological study of bending-related faulting and mantle serpentinization at the Middle America trench. Earth and Planetary Science Letters, 258(3–4): 528–542, doi: 10.1016/j.epsl.2007.04.013

Han Shuoshuo, Carbotte S M, Canales J P, et al. 2016. Seismic reflection imaging of the Juan de Fuca plate from ridge to trench: New constraints on the distribution of faulting and evolution of the crust prior to subduction. Journal of Geophysical Research, 121(3): 1849–1872

Hilde T W C. 1983. Sediment subduction versus accretion around the pacific. Tectonophysics, 99(2–4): 381–397, doi: 10.1016/0040-1951(83)90114-2

Hunter J, Watts A B. 2016. Gravity anomalies, flexure and mantle rheology seaward of circum-Pacific trenches. Geophysical Journal International, 207(1): 288–316, doi: 10.1093/gji/ggw275

Jaeger J C, Cook N G. 1979. Fundamentals of rock mechanics. London: Chapman and Hall, 513

Kanamori H. 1971. Seismological evidence for a lithospheric normal faulting-the Sanriku earthquake of 1933. Physics of the Earth and Planetary Interiors, 4(4): 289–300, doi: 10.1016/0031-9201(71)90013-6

Kao H, Chen W P. 1996. Seismicity in the outer rise-forearc region and configuration of the subducting lithosphere with special reference to the Japan Trench. Journal of Geophysical Research: Solid Earth, 101(B12): 27811–27831, doi: 10.1029/96JB01760

Key K, Constable S, Matsuno T, et al. 2012. Electromagnetic detection of plate hydration due to bending faults at the Middle America Trench. Earth and Planetary Science Letters, 351: 45–53

Kobayashi K, Nakanishi M, Tamaki K, et al. 1998. Outer slope faulting associated with the western Kuril and Japan trenches. Geophysical Journal International, 134(2): 356–372, doi: 10.1046/j.1365-246x.1998.00569.x

Lavier L L, Buck W R, Poliakov A N B. 1999. Self-consistent rolling-hinge model for the evolution of large-offset low-angle normal faults. Geology, 27(12): 1127–1130, doi: 10.1130/0091-7613(1999)027<1127:SCRHMF>2.3.CO;2

Lavier L L, Buck W R, Poliakov A N B. 2000. Factors controlling normal fault offset in an ideal brittle layer. Journal of Geophysical Research: Solid Earth, 105(B10): 23431–23442, doi: 10.1029/2000JB900108

Lay T, Ammon C J, Kanamori H, et al. 2010. The 2009 Samoa-Tonga great earthquake triggered doublet. Nature, 466(7309): 964–968, doi: 10.1038/nature09214

Lefeldt M, Ranero C R, Grevemeyer I. 2012. Seismic evidence of tectonic control on the depth of water influx into incoming oceanic plates at subduction trenches. Geochemistry, Geophysics, Geosystems, 13(5): Q05013

Masson D G. 1991. Fault patterns at outer trench walls. Marine Geophysical Researches, 13(3): 209–225, doi: 10.1007/BF00369150

Melosh H J. 1978. Dynamic support of the outer rise. Geophysical Research Letters, 5(5): 321–324, doi: 10.1029/GL005i005p00321

Naliboff J B, Billen M I, Gerya T, et al. 2013. Dynamics of outer rise faulting in oceanic - continental subduction systems. Geochemistry, Geophysics, Geosystems, 14(7): 2310–2327, doi: 10.1002/ggge.20155

Parsons B, Molnar P. 1976. The origin of outer topographic rises associated with trenches. Geophysical Journal International, 45(3): 707–712, doi: 10.1111/j.1365-246X.1976.tb06919.x

Poliakov A N B, Buck W R. 1998. Mechanics of stretching elastic-plastic-viscous layers: Applications to slow-spreading mid-ocean ridges. In: Buck W R, Delaney P T, Karson J A, et al, eds. Faulting and Magmatism at Mid-Ocean Ridges. Washington, D.C.: American Geophysical Union, 305–323

Poliakov A N B, Cundall P A, Podladchikov Y Y, et al. 1993. An explicit inertial method for the simulation of viscoelastic flow: An evaluation of elastic effects on diapiric flow in two-and three-layers models. In: Stone D B, Runcorn S K, eds. Flow and Creep in the Solar System: Observations, Modeling and Theory. Dordrecht: Springer, 175–195

Ranero C R, Morgan J P, McIntosh K, et al. 2003. Bending-related faulting and mantle serpentinization at the Middle America trench. Nature, 425(6956): 367–373, doi: 10.1038/nature01961

Ranero C, Sallares V. 2004. Geophysical evidence for hydration of the crust and mantle of the Nazca plate during bending at the north Chile Trench. Geology, 32(7): 549–552, doi: 10.1130/G20379.1

Ranero C R, Villaseñor A, Morgan J P, et al. 2005. Relationship between bend-faulting at trenches and intermediate-depth seismicity. Geochemistry, Geophysics, Geosystems, 6(12): Q12002

Ryan W B F, Carbotte S M, Coplan J O, et al. 2009. Global multi-resolution topography synthesis. Geochemistry, Geophysics, Geosystems, 10(3): Q03014

Supak S, Bohnenstiehl D R, Buck W R. 2006. Flexing is not stretching: An analogue study of flexure-induced fault populations. Earth and Planetary Science Letters, 246(1–2): 125–137, doi: 10.1016/

j.epsl.2006.03.028

Tilmann F J, Grevemeyer I, Flueh E R, et al. 2008. Seismicity in the outer rise offshore southern Chile: Indication of fluid effects in crust and mantle. Earth and Planetary Science Letters, 269(1–2): 41–55, doi: 10.1016/j.epsl.2008.01.044

Turcotte D L, Schubert G. 2014. Geodynamics. 3rd ed. Cambridge: Cambridge University Press, 156–158

Zhang Fan, Lin Jian, Zhan Wenhuan. 2014. Variations in oceanic plate bending along the Mariana Trench. Earth and Planetary Science Letters, 401: 206–214, doi: 10.1016/j.epsl.2014.05.032

Zhou Zhiyuan, Lin Jian. 2018. Elasto-plastic deformation and plate weakening due to normal faulting in the subducting plate along the Mariana Trench, Tectonophysics, 734–735, 59-68, doi: 10.1016/j.tecto.2018.04.008

Zhou Zhiyuan, Lin Jian, Behn M D, et al. 2015. Mechanism for normal faulting in the subducting plate at the Mariana Trench. Geophysical Research Letters, 42(11): 4309–4317, doi: 10.1002/2015GL063917